

RESEARCH ARTICLE

Neural-specific deletion of the focal adhesion adaptor protein paxillin slows migration speed and delays cortical layer formation

Mamunur Rashid¹, Judson Belmont¹, David Carpenter¹, Christopher E. Turner² and Eric C. Olson^{1,*}

ABSTRACT

Paxillin and Hic-5 are homologous focal adhesion adaptor proteins that coordinate cytoskeletal rearrangements in response to integrin signaling, but their role(s) in cortical development are unknown. Here, we find that Hic-5-deficient mice are postnatal viable with normal cortical layering. Mice with a neural-specific deletion of paxillin are also postnatal viable, but show evidence of a cortical neuron migration delay that is evident pre- and perinatally, but is not detected at postnatal day 35 (P35). This phenotype is not modified by Hic-5 deficiency (double knockout). Specific deletion of paxillin in postmitotic neurons using Nex-Cre-mediated recombination as well as *in utero* electroporation of a Cre-expression construct identified a cell-autonomous requirement for paxillin in migrating neurons. Paxillin-deficient neurons have shorter leading processes that exhibited multiple swellings in comparison with control. Multiphoton imaging revealed that paxillin-deficient neurons migrate ~30% slower than control neurons. This phenotype is similar to that produced by deletion of focal adhesion kinase (FAK), a signaling partner of paxillin, and suggests that paxillin and FAK function cell-autonomously to control migrating neuron morphology and speed during cortical development.

KEY WORDS: Developmental delay, Cortical development, Glial guided migration, Leading process

INTRODUCTION

Cells of the excitatory cortical neuron lineage undergo multiple transformations in shape and modes of migration as they radially (Rakic, 1972; O'Rourke et al., 1992) transit the developing cerebral cortex (Cooper, 2013; Kawachi, 2015; Kriegstein and Noctor, 2004). These transformations are tightly associated with specific extracellular environments (Franco and Müller, 2011). For example, slow-moving multipolar neurons interact with components in the intermediate zone before transitioning to bipolar neurons and migrating more rapidly along radial glial fibers that course through the developing cell-dense cortical plate (Nadarajah et al., 2001, 2003; Tabata and Nakajima, 2003; Noctor et al., 2004). During the final stage of migration, the leading process of the bipolar neuron transforms into the nascent dendrite as it enters the cell-sparse marginal zone (O'Dell et al., 2015, 2012; Olson et al., 2006; Chai et al., 2015). In many cell types, interaction with the extracellular


environment occurs at specific sites (e.g. focal adhesions, podosomes, point contacts), which serve as both physical anchors and as signaling centers that coordinate cellular responses (Zaidel-Bar et al., 2004; Block et al., 2008; Burridge et al., 1988). Focal adhesion adaptor proteins of the paxillin family are known components of these contact sites, linking extracellular receptors to the actin cytoskeleton and also regulating Rho-GTPase signaling (Brown and Turner, 2004). Although many paxillin-interacting proteins are expressed by developing cortical neurons, including $\beta 1$ -containing integrins (Cousin et al., 1997; Graus-Porta et al., 2001), focal adhesion kinase (FAK) (Menegon et al., 1999; Beggs et al., 2003; Rico et al., 2004) and integrin linked kinase (ILK) (Niewmierzycka et al., 2005), whether paxillin family adaptors are expressed in developing cortical neurons and their potential roles in cortical development are unknown.

Developing neurons are not known to express large focal adhesion complexes; instead, cultured neurons show smaller point contacts, particularly in the growth cones of some cell classes (Renaudin et al., 1999; Gomez et al., 1996). These point contacts contain phospho-paxillin and are dynamically regulated during axonal navigation. Neurons migrating along radial glial fibers also exhibit microdomains of contact (Cameron and Rakic, 1994), which contain novel adhesion molecules including connexin 43 (Cx43) and connexin 26 (Cx26) (Elias et al., 2007; Nadarajah et al., 1997), proteins that are also found in gap junctions. FAK has recently been demonstrated to interact with Cx26 and control the pace of cortical neuron migration (Valiente et al., 2011). In addition, $\beta 1$ -containing integrins, which are known to localize with paxillin in focal adhesions, are also expressed in the developing cortex and are required for normal cortical development. $\alpha 3\beta 1$ integrin (Schmid et al., 2004; Dulabon et al., 2000) may be involved in the recognition of the radial glial fiber by the migrating neuron, whereas $\alpha 5\beta 1$ integrin may be necessary for radial migration (Marchetti et al., 2010) and the initial attachment of the leading process to fibronectin localized in the marginal zone (Sekine et al., 2012). In addition, deletion of $\beta 1$ integrin in neural precursors, but not in neurons, causes pial basal lamina disruptions and a secondary cortical lamination disruption (Belvindrah et al., 2007). These findings collectively raise the possibility that paxillin or paxillin family members could have important roles in the developing cerebral cortex.

There are three members of the paxillin family of adaptor proteins: paxillin, Hic-5 (Tgfb1i1) and leupaxin (Brown and Turner, 2004). All family members share the same basic organization of multiple N-terminal leucine-rich LD motifs and multiple C-terminal zinc finger LIM domains. In paxillin itself, LIM domains 2 and 3 collectively mediate focal adhesion targeting, while the remaining LD motifs and LIM domains scaffold the assembly of a large protein complex that both links to the cytoplasmic tails of cell surface receptors (e.g. integrins, syndecan-4) to the actin cytoskeleton and coordinates signaling through the mitogen-activated protein kinase

¹Department of Neuroscience and Physiology, SUNY Upstate Medical University, 505 Irving Avenue, Syracuse, NY 13210, USA. ²Department of Cell and Developmental Biology, SUNY Upstate Medical University, 750 E Adams Street, Syracuse, NY 13210, USA.

*Author for correspondence (olsone@upstate.edu)

 M.R., 0000-0001-6768-1814; D.C., 0000-0002-9261-7168; E.C.O., 0000-0002-1545-6532

(MAPK) and small Rho-GTPase signaling pathways (Brown and Turner, 2004; Deakin and Turner, 2008; Tumbarello and Turner, 2007). More recent work has identified roles for paxillin in microtubule acetylation (via HDAC6) (Deakin and Turner, 2014), suggesting a broader cytoskeletal regulatory function(s) beyond F-actin assembly and dynamics. Hic-5 is also localized in focal adhesion, controls migration and has the ability to act as a transcriptional co-activator (Shibanuma et al., 2004). Coordinated signaling of Hic-5 and paxillin maintain the cancer cell morphology required for migration and invasion (Deakin and Turner, 2011). Leupaxin is expressed only during hematopoiesis (Lipsky et al., 1998), whereas the expression patterns of paxillin and Hic-5 in the developing cortex are unknown. Paxillin deletion is lethal by embryonic day 9.5 (E9.5) (Hagel et al., 2002), before the initiation of cortical development, whereas mice lacking Hic-5 are postnatal viable but exhibit vascular healing defects (Kim-Kaneyama et al., 2011), reduced tumor growth and metastasis (Goreczny et al., 2016). The neuroanatomy of the Hic-5-deficient mouse is, to date, not described. Thus, the developmental expression patterns of paxillin and Hic-5 in the brain, as well as the neuroanatomy of paxillin- and Hic-5-deficient mice are unknown.

In this study, we have generated and characterized paxillin conditional knockout mice, Hic-5 global knockout mice and paxillin/Hic-5 double knockout mice. We find that single and double knockout animals are postnatal viable with overtly normal neuroanatomy. However, cortical layer formation is delayed as a consequence of paxillin deletion. We find paxillin functions cell-autonomously in migrating neurons to control their morphology and migration rate.

RESULTS

Paxillin and Hic-5 expression in the developing brain

To determine spatial expression patterns of paxillin family mRNAs in the developing cortex, we performed *in situ* hybridization with digoxigenin-labeled *Pxn*, *Hic-5* and *Lpxn* antisense probes on E15.5 cortical sections of mouse brain. In the dorsal telencephalon, we found that both paxillin and Hic-5 mRNA were localized in the ventricular zone (VZ) and intermediate zone (IZ), with declining

expression in the cortical plate (CP) (Fig. 1A). In contrast, the *Lpxn* signal was comparable with the negative (*Hic-5 sense*) control. To determine paxillin, Hic-5 and leupaxin expression levels in developing excitatory neurons, we queried an existing mRNA expression data set derived from fluorescence activated cell (FAC) sorted excitatory neurons (Cameron et al., 2012). In this previous study, GFP-expressing neurons were FAC isolated from E14.5 Tg(Eomes-eGFP)Gsat embryonic mouse cortex, a line that expresses GFP specifically in the immature excitatory lineage (intermediate neural precursors and immature neurons). Microarray analysis of Eomes⁺ cells showed *Pxn* RMA (robust multichip average) at a value of 8.7, above the negative control value of 5.5 assigned from 10 retina-specific mRNA transcripts (Cameron et al., 2012). In contrast, *Hic-5* expression was lower (6.8) and *Lpxn* levels (5.9) were at the level of the negative control. For comparison, the essential adaptor protein Dab1 was expressed at 10.7 (Fig. 1B). To confirm the previous microarray analysis, mRNA was purified and reverse transcribed (RT) from Eomes-eGFP⁺ cells that were FAC isolated from E14.5 cortices ($n=3$). Quantitative polymerase chain reaction (qPCR) revealed that *Pxn* mRNA was expressed at approximately twice the levels of *Hic-5* mRNA, whereas *Lpxn* was not detected (Fig. 1C; $Pxn=1.89\pm 1.1$; $Hic-5=1.0\pm 0.48$). A query of the DeCoN transcriptome database (Molyneaux et al., 2015) independently confirms that *Pxn* and *Hic-5* are expressed by multiple classes of developing cortical excitatory neurons, including both deep layer projection neurons and upper layer callosal neurons. We next analyzed the expression level of paxillin and Hic-5 protein in lysates derived from cortices dissected at embryonic days E10-P0. Western blot analyses showed that paxillin and Hic-5 proteins were highly expressed at E13, whereas expression was downregulated by the end of corticogenesis (Fig. 1D). These findings show that both paxillin and Hic-5 are expressed by neural precursors and excitatory neurons, raising the possibility of development roles in corticogenesis.

CNS-specific deletion of paxillin and Hic-5

To avoid early embryonic lethality, paxillin floxed (*Pxn*^{F/F}) mice were generated such that exons 2-5 of paxillin gene were flanked by

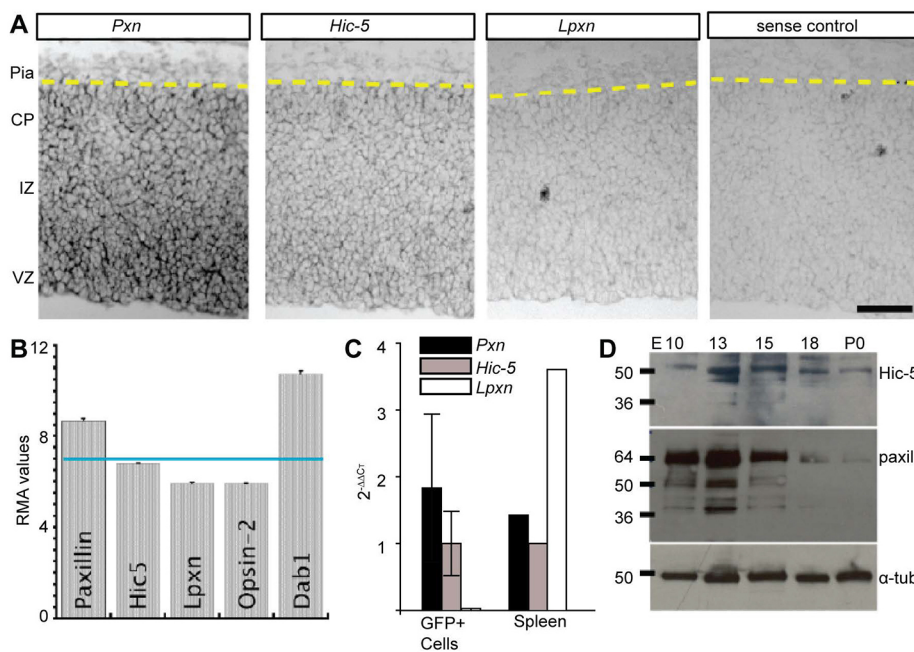


Fig. 1. Paxillin and Hic-5 are expressed in the developing cortex. (A) *In situ* hybridization of E15.5 neocortex using paxillin (*Pxn*), *Hic-5* and leupaxin (*Lpxn*) probes. *Pxn* and *Hic-5* were detected prominently in the VZ, with lower *in situ* signal in the IZ and CP. (B) Microarray analysis of immature excitatory neurons isolated by FACS from Tg(Eomes-eGFP)Gsat cortex at E14.5 (Cameron et al., 2012). *Pxn* and *Hic-5* RMA (robust multichip average) expression levels are above the expression level of *Lpxn* and eye-specific opsin 2 (not expressed). (C) RT-qPCR analysis of immature excitatory neurons (GFP⁺) isolated by FACS from Tg(Eomes-eGFP)Gsat cortex at E14.5 ($n=3$ embryos). Values were first normalized (to G6PDH) and then presented relative to *Hic-5* 2^{-ΔΔCT}. Spleen tissue ($n=1$) was used as a positive control. (D) Western blot analyses of paxillin and Hic-5 protein in the developing cortex (E10-P0). Paxillin and Hic-5 are expressed highly during corticogenesis (E13-E15) but decrease perinatally (P0). α -tubulin was used as a loading control. VZ, ventricular zone; IZ, intermediate zone; CP, cortical plate. Scale bar: 50 μ m.

engineered loxP sites (Fig. 2A). We first used *Nestin-Cre* (*Nes-Cre*) transgenic mice (Tronche et al., 1999) to specifically delete the floxed allele from the developing mouse central nervous system (*Nes-Cre:Pxn^{F/F}*). Previously, it has been reported that the *Nes-Cre*-mediated recombination event is first detected in neural precursors at E10.5 (Graus-Porta et al., 2001), at the onset of corticogenesis. To assay *Nes-Cre* dependent recombination events in the brain, we collected genomic DNA from dissected cortical tissue at E14.5 and confirmed the presence of the recombined or knockout (KO) allele (Fig. 2B). To determine whether Cre-mediated recombination eliminates paxillin protein expression, we performed western blot analysis on lysates isolated from E14.5 brain hemispheres and confirmed the profound reduction of paxillin protein in the brain (Fig. 2C). Importantly, no immunoreactive protein was detected at molecular weights lower than native paxillin (64 kDa), suggesting that the recombined allele does not generate unexpected truncated protein and is therefore a protein-null allele.

Similar to the *in situ* pattern, a paxillin immunohistochemical signal was distributed from the VZ to the CP (Fig. S1). In the CP of wild-type sections, discrete puncta of paxillin was found in the somata area and this perisomatic signal was not observed in the paxillin mutant sections. The *Nes-Cre:Pxn^{F/F}* mice were born at an expected Mendelian frequency (Table S1). Mice that lack paxillin in the brain are viable and fertile. Examination of the mutant brain at postnatal day 35 revealed no obvious neuroanatomical abnormalities compared with littermate controls (Fig. 2E,F). In

addition, there was no difference in the cortical thickness, measured from VZ to pial surface, between mutant and control (Fig. 2G; for SSs control=1465±20.8 μm; *Nes-Cre:Pxn^{F/F}*=1509.1±33.5 μm; *P*>0.05; for SSp control=1256.0±14.1 μm; *Nes-Cre:Pxn^{F/F}*=1249.4±7.0 μm; *P*>0.05). This initial examination suggests that paxillin deficiency does not dramatically disrupt gross neuroanatomy.

To determine whether *Hic-5* might compensate for paxillin deletion during cortical development, we first examined the *Hic-5*-deficient mouse. Consistent with previous reports (Kim-Kaneyama et al., 2011), we found that these independently generated (Goreczny et al., 2016) *Hic-5* knockout (*Hic-5^{-/-}*) mice were born at the expected Mendelian ratios and were fertile. Neuroanatomical evaluation revealed no obvious abnormalities compared with littermate heterozygotes. The mean neuronal positioning was unaffected in the *Hic-5^{-/-}* cortex (Fig. S2). Additionally, we performed immunoblot analysis on (E15) *Nes-Cre:Pxn^{F/F}* cortical lysate and found no difference in *Hic-5* levels compared with littermate controls (Fig. 2D). These analyses suggest that *Hic-5* is not essential for normal cortical development.

To determine whether *Hic-5* deficiency alters the cortical phenotype caused by paxillin deficiency, we generated double-knockout mice: *Nes-Cre:Pxn^{F/F}Hic-5^{-/-}* (dKO). As leupaxin is not expressed in the brain, the dKO cortex develops in the absence of all known members of the paxillin family of adaptor proteins. Similar to *Nes-Cre:Pxn^{F/F}*, dKO mice are also viable and fertile, with no overt abnormalities in the gross anatomy of the adult brain. The

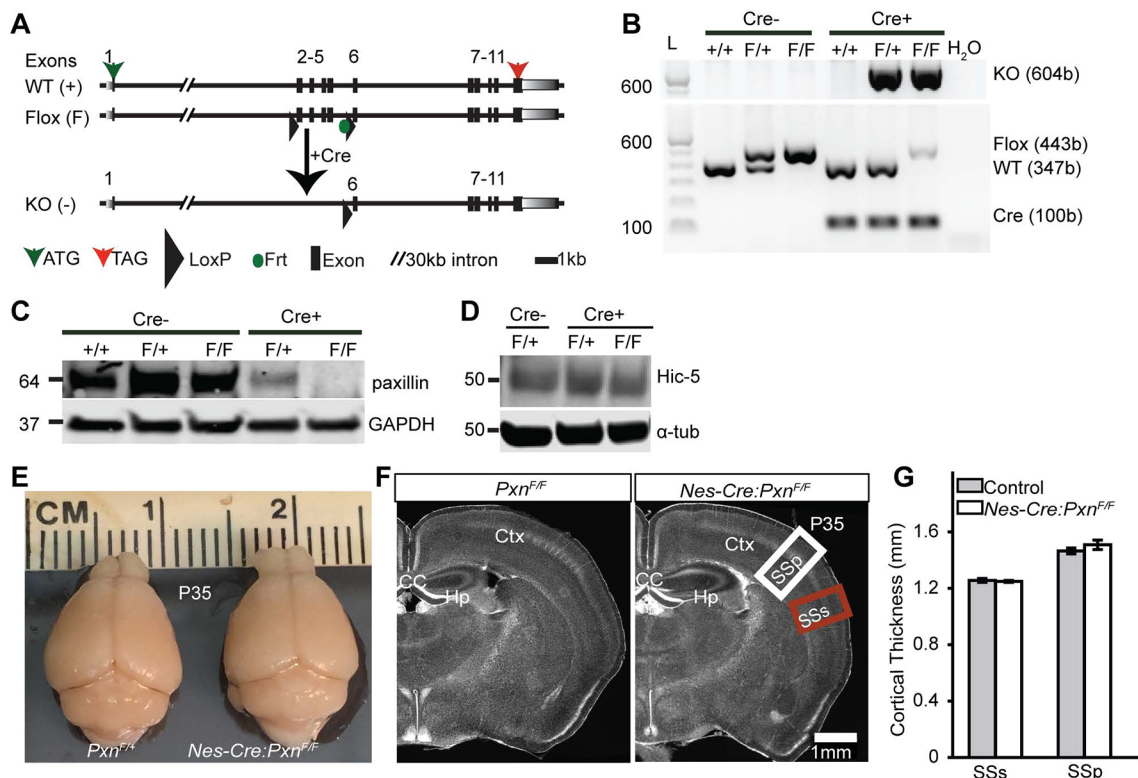


Fig. 2. Generation of the *Pxn* flox allele and neural precursor-specific deletion of paxillin by *Nes-Cre*. (A) Schematic of the *Pxn* wild-type and *Pxn* flox allele. After Cre-mediated recombination, exons 2-5 are removed creating a frameshift and multiple stop codons in exon 6. (B) Genotyping of DNA isolated from brain. Expression of the KO allele (604 bp) in the presence of Cre confirms the recombination event. The faint flox band in the presence of Cre is presumably due to unrecombined DNA from non-neural tissues, including blood vessels and meninges. (C) Western blot analysis confirming the deletion of paxillin from the mutant cortex. (D) *Hic-5* protein levels were unchanged in *Pxn*-deficient tissue. (E) Representative images of control (*Pxn^{F/+}*) and mutant (*Nes-Cre:Pxn^{F/F}*) brains at P35. (F) Coronal sections of cortex stained with Hoechst 33342 nuclear dye showing the major structures of the brain. (G) There was no difference in the cortical thicknesses of supplemental somatosensory (SSs, red box in F) or primary somatosensory cortex (SSp, white box in F) between the groups (*n*=4 per group). Error bars represent s.e.m. Data were analyzed using unpaired Student's *t*-test. Scale bar: 1 mm.

double-knockout mice were born in expected Mendelian frequencies (Table S2). A fraction (28%) of the pups generated from this cross died within a few days of birth but this was independent of genotype. The overall external appearance of the dKO brain appeared normal compared with control (Fig. S3A,B); however, the brains appeared smaller. The post-fixed brain weight of dKO was 8% smaller compared with *Hic-5*^{-/-} littermate controls (*Pxn*^{F/F}*Hic-5*^{-/-}) (Fig. S3C; control=0.49±0.03 g; dKO=0.45±0.03 g; *P*<0.001). However, after normalizing brain weight to body weight, the brain/body ratios of dKO animals were indistinguishable from the controls (Fig. S3D; control=0.027±0.002; dKO=0.030±0.001; *P*>0.05), suggesting that the brain hypoplasia was secondary to a modest overall body hypoplasia of unknown origin. We next measured the thickness of the cortex and brain areas from the rostral to the caudal region of the brain. There was no difference in the cortical thickness or brain areas between controls and the dKO (Fig. S3E,F).

Altered positioning of upper layer neurons in the paxillin mutant at P1

In many cell types, paxillin is required for the cytoskeletal rearrangements underlying cell spreading, migration (Sero et al., 2011; Deramautd et al., 2014; Hagel et al., 2002) and morphological transitions (Deakin and Turner, 2011). We hypothesized that paxillin deficiency might therefore disrupt migration with a consequential alteration of the cortical layer formation. Using coronal brain sections, we performed immunohistochemical analyses with antibodies directed against the transcription factor Cux1 that identifies upper (II–IV) cortical layers (Nieto et al., 2004), as well as antibodies directed against deep layer (V–VI)-expressed transcription factors Tbr1 (Bulfone et al., 1995; Hevner et al., 2001) and Tle4 (Yao et al., 1998; Molyneux et al., 2015). We measured the somal position of the immunolabeled neurons from the white matter and expressed that distance as fraction of total distance between the white matter and pial surface (Fig. 3A). At E19 and postnatal day 1 (P1), Cux1⁺ neurons are found in the upper layers of developing control cortices (Fig. 3B,C, Fig. S4A). Surprisingly, the mean position of the Cux1⁺ neurons was 12% deeper at E19 (Fig. S4A–C; *Pxn*^{F/F}=67.0±0.5%; *Nes-Cre:Pxn*^{F/F}=54.9±1.6%; *P*<0.001) and 11.5% deeper at P1 in the paxillin-deficient mutant cortices (Fig. 3B,C; control=75.1±1.6%; *Nes-Cre:Pxn*^{F/F}=62.9±1.4%; *P*<0.001) compared with the control groups [*Pxn*^{F/F} (WT) and *Nes-Cre:Pxn*^{F/+} (HET)]. As the control groups (WT and HET) were not different from one another in mean position, they are combined for statistical analyses and presentation (Table S3 and S4). The difference in mean position between genotypes was not due to differences in the fraction of Cux1⁺ neurons in the counting box, as these values did not differ between groups (Fig. S4D; *Pxn*^{F/F}=43.0±1.6%; *Nes-Cre:Pxn*^{F/F}=49.7±2.7%; *P*>0.05). To confirm that paxillin deficiency alters the distribution of upper-layer neurons, BrdU labeling was performed on E15.5 to target upper cortical layer neurons (Takahashi et al., 1999). Similar to the Cux1 analysis, we found a 16.3% deeper mean position of BrdU⁺ cells in the paxillin-deficient cortex when analyzed at P1 (Fig. 3D,E; *Pxn*^{F/F}=71.6±3.5%; *Nes-Cre:Pxn*^{F/F}=55.3±1.5%; *P*<0.05). In contrast, developing deep layer neurons did not show malpositioning when analyzed at P1. Both Tbr1⁺ (Fig. 3G; *Pxn*^{F/F}=25.9±1.2%; *Nes-Cre:Pxn*^{F/F}=25.6±2.1%; see also Fig. S1C) and Tle4⁺ neurons (Fig. 3F,G; *Pxn*^{F/F}=30.3±2.0%; *Nes-Cre:Pxn*^{F/F}=29.8±2.2%; *P*>0.05) showed no difference in position between genotypes.

While FAK conditional knockout mice showed a similar migration delay phenotype (Valiente et al., 2011), we did not find

changes in the level of phospho-FAK (pFAK) or total FAK between genotypes (Fig. S5A–C). Similarly, paxillin was recently found to regulate microtubule acetylation by inhibiting HDAC6 (Deakin and Turner, 2014), but we did not observe any difference in the level of acetylated tubulin in the mutants (Fig. S5D).

To determine whether *Hic-5* may provide functional redundancy for paxillin, we examined the *Hic-5*^{-/-} cortices and found no difference in the positioning of Cux1⁺ neurons in mutant and controls (Fig. S4A–C). We next analyzed the distribution of layer-specific molecular markers of the dKO (*Nes-Cre:Pxn*^{F/F}*Hic-5*^{-/-}) cortex. We found that the dKO has a lamination defect similar to paxillin single knockout: the normalized mean position of Cux1⁺ neurons were 10% deeper in the dKO cortex compared with littermate controls at P0 (Fig. 4A,B; control=75±1.4%; dKO=65±2.9%; *P*<0.05). The mean positions of deep Tbr1⁺ (Fig. 4D; control=43±2.2%; dKO=42±2.3%; *P*>0.05; see also Fig. S1D), Tle4⁺ (Fig. 4C,D; control=34.33±1.1%; dKO=34.7±1.1%; *P*>0.05) and Ctip2⁺ (Fig. 4C,D; control=56.8±2.6%; dKO=57.0±2.0%; *P*>0.05) neurons were indistinguishable between groups. Altogether, these findings suggest that, among the paxillin family adaptors, paxillin is essential for normal cortical positioning.

Normal positioning of upper layer neurons in paxillin mutants at P35

The ectopic deep location of the Cux1⁺ neurons P1 might be produced by premature migration arrest or might be due to a migration delay, as was found with FAK deficiency (Valiente et al., 2011). We therefore analyzed cortical sections at P35 and could no longer detect any difference in mean positioning of the Cux1⁺ neurons in any genotype (Fig. 3H,I; control=60.1±1.2%; *Nes-Cre:Pxn*^{F/F}=58.0±1.7%; *P*>0.05). This suggests the ectopic positioning was due to a migration delay, rather than inappropriate migration arrest. Similar to the P1 cortex, there was no difference in the mean positioning of the Tbr1⁺ (Fig. 3K; control=36.1±1.9%; *Nes-Cre:Pxn*^{F/F}=40.8±3.3%; *P*>0.05; see also Fig. S1F) and Tle4⁺ (Fig. 3J,K; control=21.4±0.6%; *Nes-Cre:Pxn*^{F/F}=21.0±0.7%; *P*>0.05) neurons between the groups. Like the paxillin mutant, the mean positions of upper and deeper layers was indistinguishable between dKO and littermate controls when analyzed at P35 (Fig. 4E,F; for Cux1: control=65±1.8%; dKO=64±1.2%; *P*>0.05; Fig. 4G,H; for Tbr1: control=43±3.4%; dKO=46±1.3%; *P*>0.05; see also Fig. S1G; for Tle4: control=20.5±0.5%; dKO=19.7±0.7%; *P*>0.05). Together these findings indicate paxillin deficiency does not cause a migration arrest but rather delays neuronal positioning.

Migrating neuron-specific deletion of paxillin alters positioning of upper layer neurons at P1

Nes-Cre-mediated recombination occurs in the radial glia (neural precursors) and their descendant cells (neurons and glia) (Malatesta et al., 2000; Graus-Porta et al., 2001). The radial glial cell itself can span the entire width of cerebral cortex and is the substrate for radially directed neuronal migration. In addition, disruptions of the radial glial endfeet by deletion of β1 integrin or integrin-linked kinase (ILK) were associated with disrupted cortical positioning (Graus-Porta et al., 2001; Niewmierzycka et al., 2005). Thus, the altered positioning of paxillin-deficient neurons could be due to paxillin loss in either the neurons or the radial glial cells or both. To determine whether the observed phenotype is due to paxillin loss in the migrating neurons, we used a *NEX-Cre*-mediated genetic approach to specifically delete paxillin from postmitotic migrating neurons (Wu et al., 2005; Bartholomä and Nave, 1994). Similar to the phenotype of the *Nes-Cre:Pxn*^{F/F} mice, the positioning of the

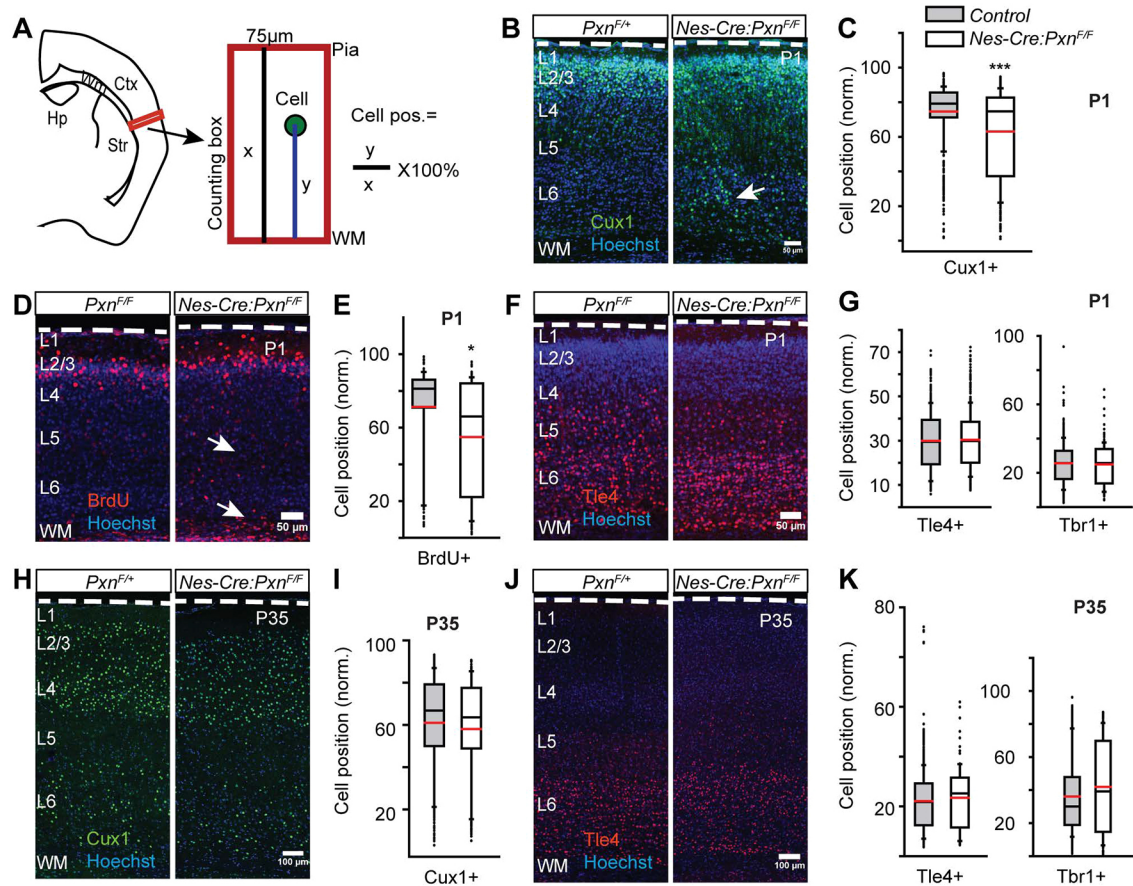


Fig. 3. Neural precursor-specific deletion of paxillin delays upper layer neuronal positioning. (A) Schematic of neuronal positioning analyses within a defined area in lateral neocortex (box). Neuronal positions (y) were measured from the underlying white matter (WM), normalized to the total thickness of the cortical wall (x), and expressed as a percentage. (B-G) Neuronal position at P1. (B) Representative images of P1 littermate controls ($Pxn^{F/F}$) and mutants ($Nes-Cre:Pxn^{F/F}$) immunostained for Cux1 (green). More Cux1⁺ neurons were found in ectopic deep positions (arrow) in the mutant cortex compared with littermate controls. (C) Box-and-whisker plot showing a broad distribution of Cux1⁺ neurons in the mutant cortices. The mean position of Cux1⁺ neurons was significantly deeper in the mutant cortex [$n=7$ for control (4 $Pxn^{F/F}$ and 3 $Nes-Cre:Pxn^{F/F}$) and $n=5$ for $Nes-Cre:Pxn^{F/F}$]. (D) Representative images of BrdU⁺ (injected at E15.5) neurons (red) at P1 showing ectopic BrdU⁺ cells in the deep cortex (arrows). (E) Box-and-whisker plot showing the distribution of BrdU⁺ neurons in the mutant cortices. The mean position of BrdU⁺ neurons was significantly deeper in the mutant cortex [$n=3$ for $Pxn^{F/F}$ (control) and $n=4$ for $Nes-Cre:Pxn^{F/F}$ (mutant)]. (F) Representative images of Tle4⁺ neurons (red) at P1. (G) Box-and-whisker plot distribution of Tle4⁺ neurons and Tbr1⁺ neurons. There was no difference in the mean position of Tle4⁺ [$n=3$ for $Pxn^{F/F}$ (control) and $n=4$ for $Nes-Cre:Pxn^{F/F}$ (mutant)] neurons and no difference between Tbr1⁺ [$n=4$ $Pxn^{F/F}$, $n=3$ $Nes-Cre:Pxn^{F/F}$ (controls) and $n=5$ for $Nes-Cre:Pxn^{F/F}$ (mutant)] neurons. (H-K) Neuronal position analysis in P35 cortex. (H) Representative images of P35 littermate control ($Pxn^{F/F}$) and mutant ($Nes-Cre:Pxn^{F/F}$) neurons immunostained for Cux1 (green). (I) Distribution of Cux1⁺ neurons. No difference in the mean position of Cux1⁺ neurons was detected between genotypes [$n=7$ for control ($n=4$ $Pxn^{F/F}$ and $n=3$ $Nes-Cre:Pxn^{F/F}$) and $n=4$ for $Nes-Cre:Pxn^{F/F}$ (mutant)]. (J) Representative image of Tle4⁺ (red) neurons at P35. (K) Distribution of Tle4⁺ and Tbr1⁺ neurons. No difference in the mean position of either Tle4⁺ [$n=9$ in control ($n=5$ $Pxn^{F/F}$ and $n=4$ $Nes-Cre:Pxn^{F/F}$), $n=5$ in $Nes-Cre:Pxn^{F/F}$ (mutant)] or Tbr1⁺ [$n=6$ in control ($n=3$ $Pxn^{F/F}$ and $n=3$ $Nes-Cre:Pxn^{F/F}$), $n=4$ in $Nes-Cre:Pxn^{F/F}$ (mutant)] neurons was detected between genotypes. Dashed white lines outline the pial surface. Data were analyzed using unpaired Student's t -test. * $P<0.05$, *** $P<0.001$. Scale bars: 50 μ m in B,D,F; 100 μ m in H,J.

Cux1⁺ neurons was 11.6% ectopically deeper in the cortex of $Nes-Cre:Pxn^{F/F}$ mice compared with littermate controls (Fig. 5A,B; $Pxn^{F/F}=79\pm 0.9\%$; $Nes-Cre:Pxn^{F/F}=67.4\pm 0.8\%$; $P<0.001$). There was no difference in the mean positioning of Tbr1⁺, Tle4⁺ or Ctip2⁺ deep layer cortical neurons in the $Nes-Cre:Pxn^{F/F}$ cortex compared with littermate controls (Fig. 5C,D; for Tbr1: $Pxn^{F/F}=36.3\pm 0.28\%$; $Nes-Cre:Pxn^{F/F}=36.0\pm 0.3\%$; $P>0.05$; see also Fig. S1; for Tle4: $Pxn^{F/F}=31.1\pm 0.2\%$; $Nes-Cre:Pxn^{F/F}=32.4\pm 1.6\%$; $P>0.05$). These findings suggest that paxillin function in neurons (not precursors) is required for correct cellular positioning.

Cell-autonomous deletion of paxillin disrupts the morphology of migrating neurons

To determine the cell-autonomous phenotype caused by paxillin deletion, we performed *in utero* electroporation (IUEP) of pCAG-

Cre:GFP (Matsuda and Cepko, 2007) and pCAG-tdTomato into $Pxn^{F/+}$ (controls), $Pxn^{F/F}$ (single KO) or $Pxn^{F/F}Hic-5^{-/-}$ (dKO) embryos. The IUEPs were performed at E15 to target upper layer neurons and analyzed postnatally, allowing the cells to reach developing layer II/III (Takahashi et al., 1999). We measured the position of labeled neurons from the ventricular surface. We found that Cre-electroporated paxillin-deficient neurons are found 20% deeper in the cortex compared with the littermate controls (Fig. 6A-C; $Pxn^{F/+}=80\pm 0.9\%$; $Pxn^{F/F}=60\pm 4.2\%$; $P<0.05$). We next electroporated either pCAG-tdTom (control group) and pCAG-tdTom+pCAG-Cre:GFP (dKO group) into E15.5 $Pxn^{F/F}Hic-5^{-/-}$ embryos to assess the consequence of cell-autonomous paxillin deficiency in the context of global *Hic-5* deficiency. As with cell-autonomous paxillin deficiency, the mean position of Cre:GFP electroporated dKO neurons was 19% deeper compared with the

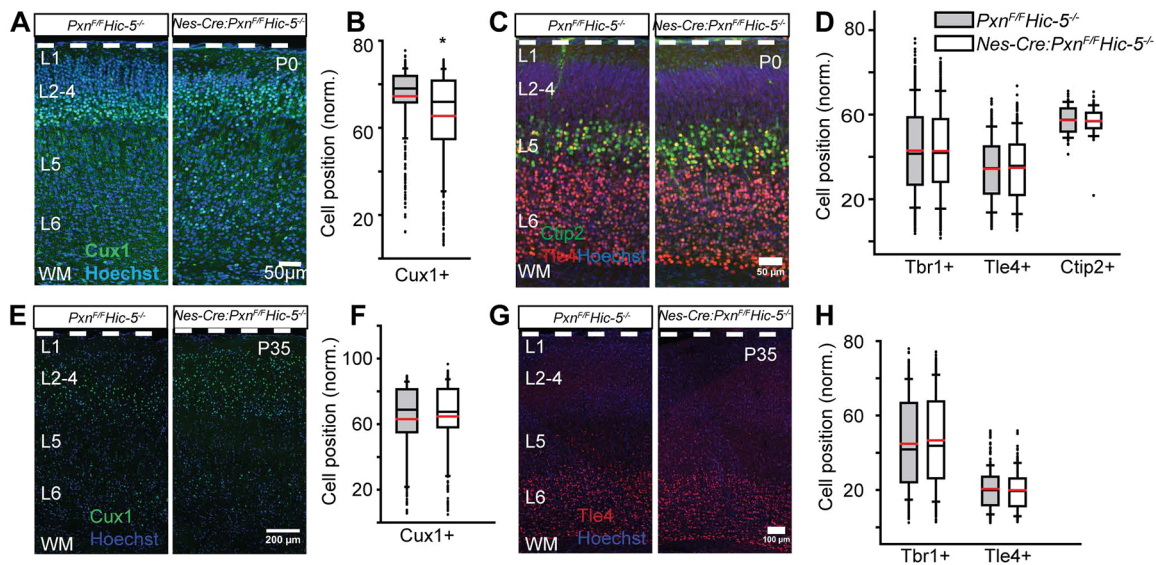


Fig. 4. Combined *Hic-5* deficiency with paxillin deficiency (dKO) produces an upper layer neuronal positioning defect similar to that observed with paxillin deficiency alone. (A–D) Neuronal position analysis of P0 cortex. (A) Representative images of P0 littermate control and dKO immunostained for Cux1 (green). More Cux1⁺ neurons were found in ectopic deep positions in the dKO cortex compared with littermate controls. (B) Box-and-whisker plot distribution of Cux1⁺ neurons showing a broad distribution of Cux1⁺ neurons in the dKO cortex. Mean position of Cux1⁺ neurons is significantly deeper in the dKO cortex ($n=5$ per group). (C) Representative images of Tle4⁺ (red) and Ctip2 (green) neurons at P0. (D) Distribution of Tbr1⁺ ($n=5$), Tle4⁺ ($n=4$) and Ctip2⁺ ($n=3$) neurons. No difference in the mean positions of the markers was found between genotypes. (E–H) Neuronal position analysis of P35 cortex. (E) Representative images of P35 littermate control and dKO immunostained for Cux1 (green). (F) Distribution of Cux1⁺ neurons. There was no difference in the mean position of Cux1⁺ neurons between genotypes ($n=6$). (G) Representative image of Tle4⁺ (red) neurons at P35. (H) Distribution of Tbr1⁺ ($n=6$) and Tle4⁺ ($n=4$) neurons. There was no difference in the mean position of either Tbr1⁺ or Tle4⁺ neurons between genotypes. Data were analyzed using unpaired Student's *t*-test. * $P<0.05$. Scale bars: 50 μm in A,C; 200 μm in E; 100 μm in G.

Hic-5^{-/-} control (Fig. 7A–C; tdTom=72±1.7%; tdTom+Cre: GFP=53±0.8%; $P<0.001$). This finding suggests that the phenotype found in the *Nes-Cre:Pxn*^{F/F} mutants at P1 is due to cell-autonomous loss of paxillin.

Migrating neurons have a characteristic morphology with a monopolar leading process that navigates the neuron along the radial glial fiber. To explore the possibility that paxillin deficiency alters migrating neuron morphology, we acquired high-resolution confocal *z*-series of migrating neurons that, based on their position in the deep cortical plate, would likely be undergoing glial-guided locomotory migration. Paxillin-deficient neurons

exhibited a 24% shorter leading process compared with littermate controls (Fig. 6F; *Pxn*^{F/+}=88±5.1 μm ; *Pxn*^{F/F}=67±3.4 μm , $P<0.01$). Similarly, cell-autonomous dKO neurons had significantly 37% shorter leading processes compared with littermate controls (Fig. 7E,F; control=76±3.4 μm ; dKO=48±1.9 μm ; $P<0.0001$). Additionally, the leading processes of single and dKO neurons exhibit multiple swellings compared with control neurons (Fig. 6G; *Pxn*^{F/+}=1.2±0.16; *Pxn*^{F/F}=2.4±0.2; $P<0.001$) and (Fig. 7G; control=1.16±0.1, dKO=2.4±0.2; $P<0.0001$). However, the number of branches per leading process was indistinguishable between the groups (Fig. 6H; *Pxn*^{F/+}=0.30±0.1; *Pxn*^{F/F}=0.36±0.2;

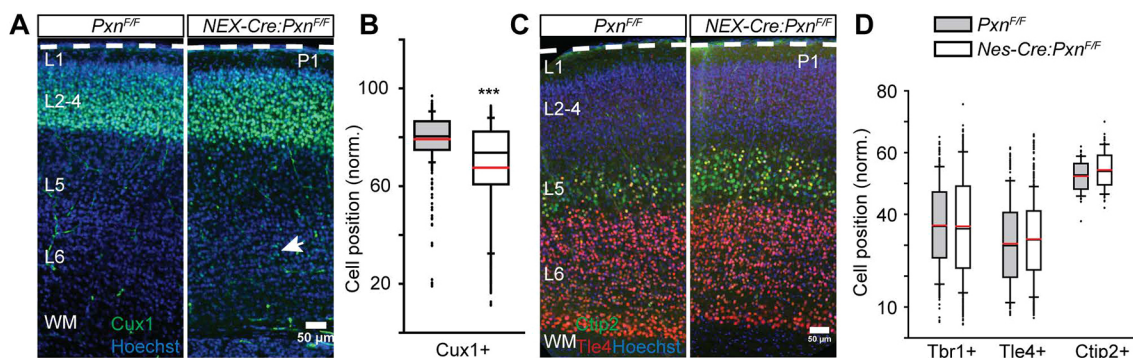


Fig. 5. Paxillin deficiency in post-mitotic neurons disrupts neuronal positioning. (A) Representative sections of littermate control (*Pxn*^{F/F}) and mutant (*NEX-Cre:Pxn*^{F/F}), with a conditional deletion of paxillin in post-mitotic immature neurons, were immunostained for Cux1 (green). More Cux1⁺ neurons were found in ectopic deep positions in the mutant cortex (arrow). (B) Box-and-whisker plot distribution of positions of Cux1⁺ neurons. The mutant showed a broader distribution compared with littermate controls. The mean position of Cux1⁺ neurons was significantly deeper in the mutant cortex ($n=3$ in *Pxn*^{F/F} and $n=4$ in *NEX-Cre:Pxn*^{F/F}). (C) Representative images of Tle4⁺ (red) and Ctip2⁺ (green) neurons. (D) Distribution of Tbr1⁺ ($n=3$ in *Pxn*^{F/F} and $n=4$ in *NEX-Cre:Pxn*^{F/F}), Tle4⁺ ($n=3$ in *Pxn*^{F/F} and $n=4$ in *NEX-Cre:Pxn*^{F/F}) and Ctip2⁺ ($n=3$ in *Pxn*^{F/F} and $n=4$ in *NEX-Cre:Pxn*^{F/F}) neurons. There was no difference in the mean positions of the Tbr1⁺, Tle4⁺ and Ctip2⁺ neurons between the genotypes. *** $P<0.001$. Scale bars: 50 μm .

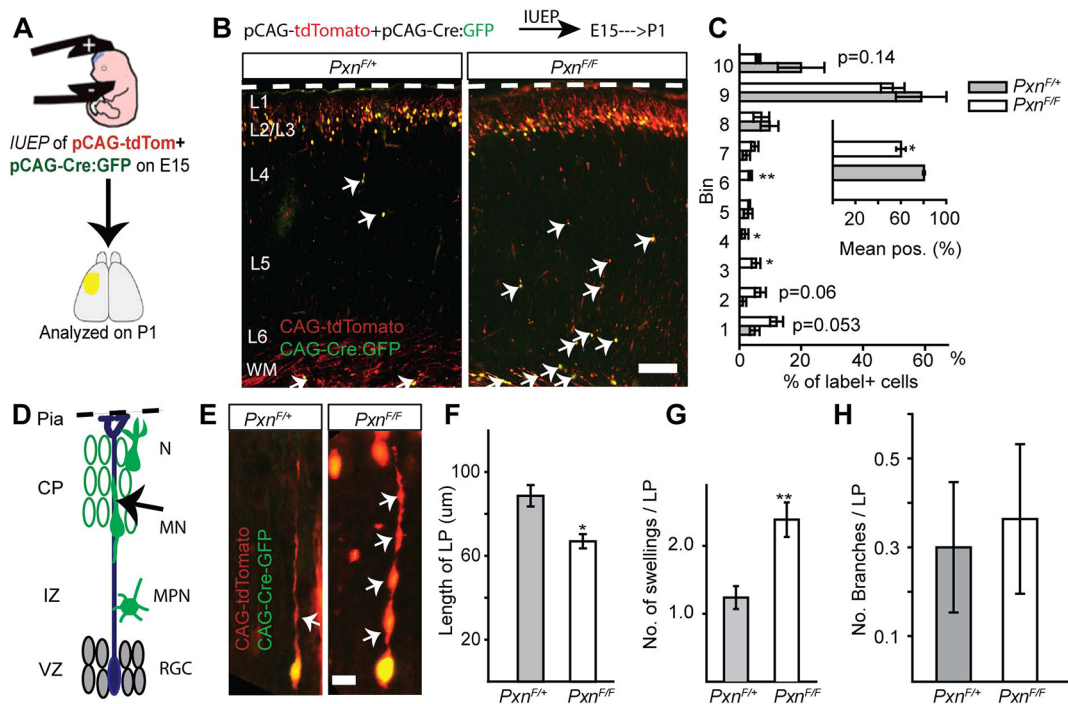


Fig. 6. Cell-autonomous deletion of paxillin alters neuronal positioning and morphology. (A) *In utero* electroporation of pCAG-tdTomato+pCAG-Cre:GFP into $Pxn^{F/+}$ (control) or $Pxn^{F/F}$ (paxillin-deficient) was performed at E15. (B) Representative image of control and paxillin-deficient neurons analyzed at P1. (C) Analysis of cell position across the cortical wall by bins (bin 1 includes WM and bin 10 includes L1). The mean cell position of the paxillin-deficient group is 20% deeper than control. (D) Schematic of radial migration and a bipolar migrating neuron (arrow) analyzed in the cortical plate (CP). (E) A control ($Pxn^{F/+}$) migrating neuron with an extended leading process (left panel). Cre-mediated deletion of paxillin shortened and increased the number of swellings (arrows) in the leading process (right panel). (F) Quantification of leading process lengths ($n=15$ cells per group). (G) Quantification of leading process swellings ($n=21$ cells for $Pxn^{F/+}$, $n=26$ cells for $Pxn^{F/F}$). (H) The number of leading process branches was indistinguishable between the groups ($n=20$ cells for $Pxn^{F/+}$, $n=22$ cells for $Pxn^{F/F}$). CP, cortical plate; IZ, intermediate zone; WM, white matter; VZ, ventricular zone; RGC, radial glial cells; MPN, multipolar neurons; MN, migrating neurons; N, differentiated neurons. * $P<0.05$, ** $P<0.01$. Scale bars: 100 μm in B; 10 μm in E.

$P>0.05$). Thus, migrating neurons with cell-autonomous deficiency in paxillin have a similar phenotype to neurons deficient in focal adhesion kinase (FAK), with increased leading process dilations, and a shortened leading process.

Paxillin-deficient neurons migrate slowly

The observation that deep layer neuron position is unaffected in the mutant could argue for differences in paxillin-dependence for deep and upper layer cortical neurons. Alternatively, deep layer positioning defects in the mutant may no longer be apparent at P1 but might be detected at earlier developmental time points. To assay for deep layer neuron position, we examined neuronal position at E16 using both Tbr1 and Bcl11a (Ctip1) as immunohistochemical markers. Tbr1⁺ protein is strongly expressed by the neuron upon entry into CP (Englund et al., 2005), which limits the detection of ectopic neurons to the CP. In contrast, Bcl11a (Ctip1), a zinc-finger family transcription factor, is expressed by migrating neurons in the upper IZ and in the CP (Wiegrefe et al., 2015). Using this approach, we found that the mean position of Ctip1⁺ neurons was 4.5% deeper in the mutant cortex (Fig. 8A,B; $Pxn^{F/F}=66.3\pm 0.9\%$; $Nes-Cre:Pxn^{F/F}=61.8\pm 0.8\%$; $P<0.05$). BrdU birthdating performed at E12.5 and analyzed at E14.5 confirmed that the mean position of early born neurons is 4.7% deeper in the mutant cortex (Fig. 8C,D; $Pxn^{F/F}=53.1\pm 1.8\%$; $Nes-Cre:Pxn^{F/F}=48.4\pm 0.9\%$; $P<0.05$). These results indicate that paxillin deletion also subtly alters deep layer neuronal positioning.

To assess the migration behavior of paxillin-deficient neurons, we performed multiphoton imaging of migrating neurons in whole-

hemisphere explants (Nichols et al., 2013; O'Dell et al., 2015). Prospective deep layer neurons were electroporated with CAG-tdTomato plasmid on E13 and imaged 2 days later as they approached the MZ and completed migration. Z-series were acquired at 10 min sampling intervals for a period of 4 h. Quantification of somal movements revealed that paxillin-deficient neurons showed a 32% slower migration rate compared with the littermate controls ($Pxn^{F/F}=43.1\pm 4.3 \mu\text{m h}^{-1}$; $Nes-Cre:Pxn^{F/F}=29.1\pm 1.7 \mu\text{m h}^{-1}$, $P<0.01$) (Fig. 8D,E). Thus, the imaging study demonstrates that paxillin is required for normal migration speed.

DISCUSSION

There are multiple adhesion systems that underlie neuronal migratory behavior, including cadherins (Jossin and Cooper, 2011; Franco et al., 2011; Stocker and Chenn, 2015), gap junction based adhesions (Valiente et al., 2011; Elias et al., 2007) and integrins (Schmid and Anton, 2003). The role of integrin-based adhesion complexes in migrating neurons *in vivo* is unclear. Deletion of $\beta 1$ -integrin and a subset of α -integrin partners has been performed with contrasting results: deletion of the $\alpha 3$ integrin retards radial migration and causes aberrant cytoskeletal dynamics in the early cortex (Schmid et al., 2004; Anton et al., 1999; Dulabon et al., 2000). Similarly, conditional deletion of $\alpha 5$ integrin also perturbs radial migration (Marchetti et al., 2010) and $\alpha 5\beta 1$ was recently shown to promote the final stage of migration (terminal translocation) to the marginal zone (Sekine et al., 2012). However, precursor and neuron-specific deletion of $\beta 1$ -integrin, which should

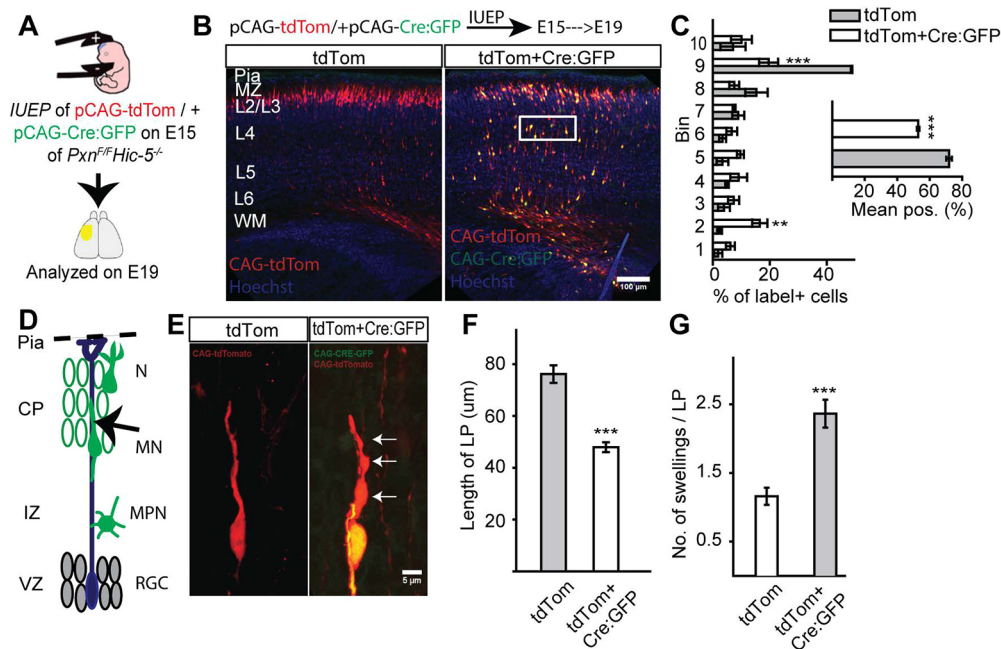


Fig. 7. Cell-autonomous deletion of paxillin in *Hic-5*^{-/-} cortex alters neuronal positioning and morphology. (A) *In utero* electroporation of pCAG-tdTomato±pCAG-Cre:GFP into *Hic-5*^{-/-}*Pxn1*^{F/F} embryos was performed at E15. (B) Representative images of control (CAG-tdTom group) and dKO (CAG-tdTom+CAG-Cre:GFP group) neurons analyzed at E19. (C) Analysis of cell position across the cortical wall by bins (bin 1 includes WM and bin 10 includes L1). The mean cell position of the dKO group is 19% deeper than control. (D) Schematic of radial migration and a bipolar migrating neuron (arrow) analyzed in the cortical plate (CP). (E) A control (*Hic-5*^{-/-}*Pxn1*^{F/F}) migrating neuron with an extended leading process (left panel). Cre-mediated deletion of paxillin shortened and increased the number of swellings (arrows) in the leading process of a dKO neuron (right panel). (F) Quantification of leading process lengths (*n*=20 per group). (G) Quantification of leading process swellings (*n*=25 cells for control; *n*=22 cells for mutant). CP, cortical plate; IZ, intermediate zone; WM, white matter; VZ, ventricular zone; RGC, radial glial cells; MPN, multipolar neurons; MN, migrating neurons; N, differentiated neurons. ***P*<0.01, ****P*<0.001. Scale bars: 100 μm in B; 5 μm in E.

ablate all β1-containing integrin dimers including α3β1 and α5β1, revealed that β1-containing integrins are required in radial glial precursors (Graus-Porta et al., 2001) but not neurons for normal cerebral cortex development (Belvindrah et al., 2007). β1-integrin deficiency in radial glial precursors leads to a disruption of the basal lamina at the pial surface of the developing brain and a resulting undulating cortical layering associated with breaches in the meningeal fibroblast layer.

Contrasting results were also observed with FAK deletion. Early studies showed a role for FAK in basal lamina formation and maintenance by the meningeal fibroblasts. FAK deletion also disrupted neuronal dendrite formation, but did not appear to alter cortical lamination, implying little or no role in migration itself (Beggs et al., 2003). However, the more recent analyses revealed an additional cell-autonomous function for FAK in regulating the morphology and rate of upper cortical layer neuron migration along radial glial fibers (Valiente et al., 2011). Importantly, the cellular malpositioning caused by FAK deficiency was transitory, present in the perinatal period, but largely resolved by P7.

Our analysis of the paxillin-deficient cortices is largely consistent with this latter study: paxillin deficiency in radial glial precursors caused a migration delay that was observed perinatally but absent by P35. Conditional deletion in post-mitotic neurons caused a similar migration and morphology phenotype, as did cell-autonomous deletion by IUEP. Paxillin-deficient migrating neurons had shorter leading processes that exhibited a larger number of swellings than control, an observation consistent with FAK-deficient phenotype. The cause of these additional swellings is unknown, and might be due to altered cytoskeletal integrity or signaling. For example,

integrin αIIbβ3 signaling can modulate membrane swellings via a sodium-proton exchanger (NHE1) and the sodium calcium exchanger (NCX1) that localize to the membrane swelling (Yi et al., 2012). Although these morphological and migrational deficits were identified in glial-associated locomotory neurons in the mid and deep cortical plate, our whole-hemisphere explant imaging approach focuses our analyses on migrating neurons in the mid and upper cortical plate. As we could not reliably determine whether migrating neurons were associated with a glial fiber, we cannot exclude the possibility that translocative (glial independent) migration, as well as locomotory (glial-guided) migration (Nadarajah et al., 2001), are disrupted by paxillin deficiency.

The gap junction proteins Cx26 and Cx43 (Elias et al., 2007; Fushiki et al., 2003) are localized in the contact points between the migrating neurons and radial glia. Acute downregulation of these gap junction proteins impaired radial migration of cortical neurons. Interestingly, gap junction properties of Cx26/Cx43 are not required for migration; instead, Cx26/Cx43 form an adhesive interaction between the neurons and radial glial fibers. Importantly, FAK was required for Cx26-mediated adhesion and full-length FAK could rescue adhesion as expected, but FAK that lacked the paxillin interaction domain could not rescue deficiency. Thus, paxillin/FAK may regulate Cx26 puncta assembly at contact sites between migrating neurons and their radial glial substrate (Valiente et al., 2011).

A branched leading process is associated with migration pauses and arrests (Nadarajah et al., 2001; O'Dell et al., 2015), thus additional branching could potentially explain the migration delay. However, in contrast to the prior FAK study, we did not observe

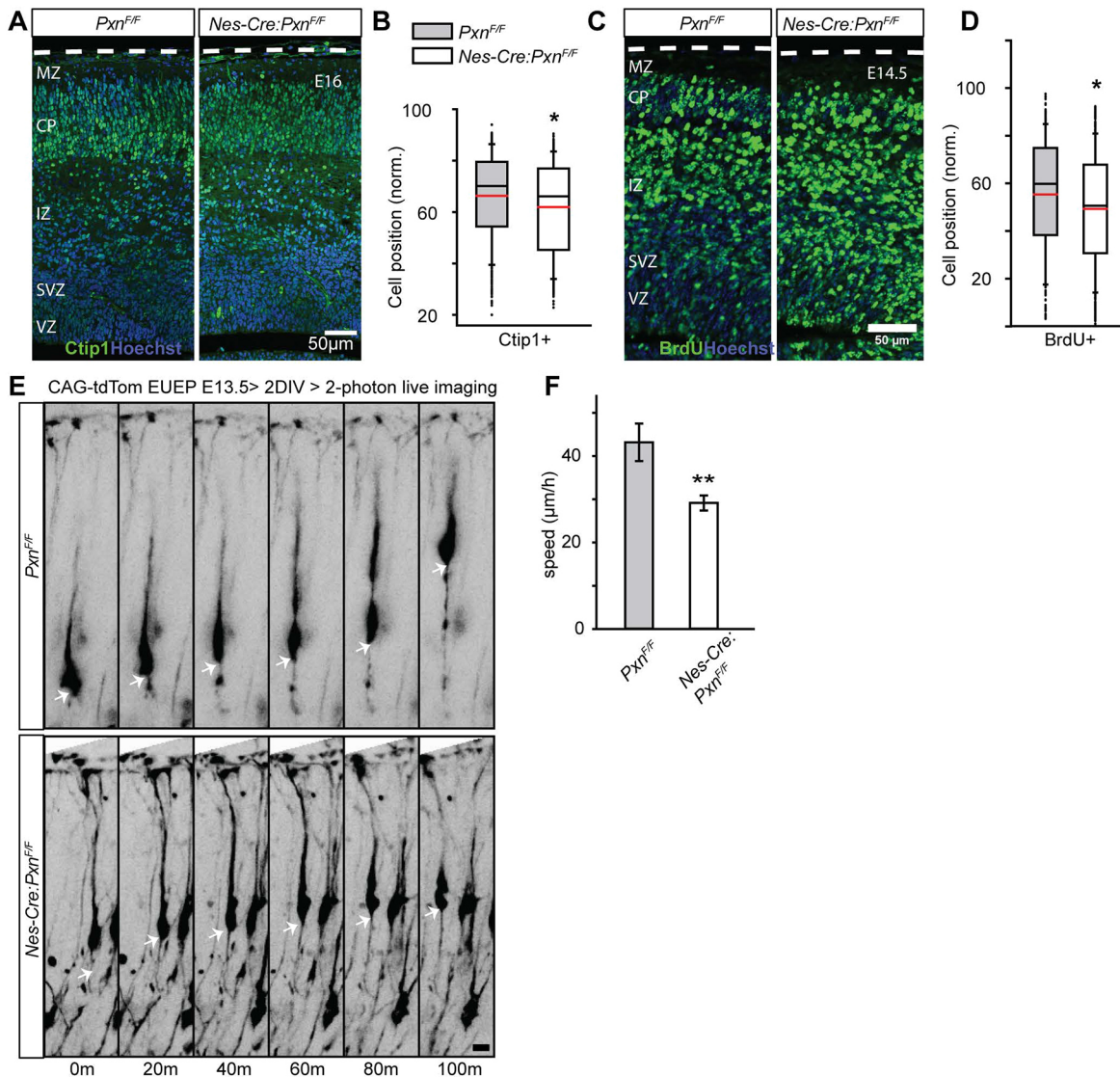


Fig. 8. Paxillin-deficient mutant neurons migrate slowly. (A) Representative images of littermate control and *Nes-Cre:Pxn^{F/F}* paxillin-deficient cortical sections immunostained for Ctip1 (green) at E16. (B) Box-and-whisker plot distribution of Ctip1⁺ neurons. The mean position of Ctip1⁺ neurons was 4.5% deeper in the paxillin mutant ($n=3$ /group). (C) Representative images of BrdU⁺ (injected at E12.5) neurons (red) at E14.5 showing ectopic BrdU positioning in the deep cortex. (D) Box-and-whisker plot showing a broad distribution of BrdU⁺ neurons in the mutant cortices. The mean position of BrdU⁺ neurons was significantly deeper in the mutant cortex ($n=4$ in *Pxn^{F/F}*, $n=5$ in *Nes-Cre:Pxn^{F/F}*). (E) Multiphoton images GFP-labeled neurons in whole hemisphere explants from *Pxn^{F/F}* (control) and *Nes-Cre:Pxn^{F/F}* (mutant) embryos. Arrows show the position of a single neuronal soma over time. (F) Quantification of speed of migrating neurons ($n=12$ cells per group from three mutant and three control explants). * $P<0.05$, ** $P<0.01$. Scale bars: 50 μm in A,C; 10 μm in E.

obvious abnormal branching at the leading process that was found in FAK-deficient neurons (Valiente et al., 2011). In addition, we were unable to detect a disruption of Cx26 localization in the absence of paxillin (not shown). Although these distinctions might represent methodological differences in the studies, it is also possible that FAK-paxillin interactions mediate the leading process morphology and migration rate, whereas FAK-Cx26 interactions regulate branching patterns.

Many of the human mutations that cause congenital cortical malformation affect microtubule proteins or microtubule regulatory proteins. Mutations in multiple tubulin genes cause a broad spectrum of cortical malformations from severe lissencephaly to more-restricted focal polymicrogyria, and are collectively called tubulinopathies (Bahi-Buisson et al., 2014). Additionally, mutations that disrupt microtubule regulatory proteins, including

Lis1 (Lo Nigro et al., 1997; Dobyns et al., 1993) and doublecortin (DCX) (Gleeson et al., 1998; des Portes et al., 1998), produce severe lissencephalies. The mechanism by which FAK-paxillin regulates neuronal migration is not understood but there is a possibility that a common effector involves regulation of microtubule stabilization. The C-terminal focal adhesion targeting (FAT) domain of FAK binds paxillin (Hildebrand et al., 1995), allowing FAK to phosphorylate paxillin at Y31 and Y118 (Bellis et al., 1995; Schaller and Parsons, 1995). Phosphorylated paxillin further recruits SH2 domain-containing adaptor proteins such as Crk and CrkL, which, in turn, recruit and coordinate small GTPases (Birge et al., 1993; Salgia et al., 1995). A dominant-negative form of Rac1 inhibits neuronal migration (Kawauchi et al., 2003), whereas migration is delayed in the Rac1 conditional knockout mouse (Chen et al., 2007; Tahirovic et al., 2010). Interestingly, one of the

downstream factors of the Rac1 pathway is Jun N-terminal kinase (JNK), which is also required for neuronal migration and leading process formation (Kawauchi et al., 2003). JNK phosphorylates microtubules associated with the protein DCX (Gdalyahu et al., 2004) and MAP1B (Kawauchi et al., 2005), as well as paxillin at S178 (Miyamoto et al., 2012). Thus, a model emerges in which paxillin and FAK could function to regulate small GTPase activity, leading to JNK activation and the phosphorylation and modification of microtubule stabilizing proteins.

The subtlety of the cortical phenotype of the *Hic-5*/paxillin double KO is surprising given the importance of this family of proteins in many forms of migration and cellular motility. The double KOs are viable and do not show dramatic alterations in postnatal brain structure. However, more-subtle disruptions may be present: for example, paxillin tyrosine phosphorylation is involved in *Xenopus laevis* axonal growth cone extension and navigation (Robles and Gomez, 2006; Myers and Gomez, 2011). Although the major axonal pathways (e.g. callosal projections) form in the paxillin mutant, whether the detailed axonal projection patterns are disrupted is unknown, and will require further analyses. Similarly, the structure of the dendrite and synaptic functionality of the mutant has not been determined. For example, long-term potentiation (LTP), the synaptic change associated with memory encoding in the hippocampus, is perturbed by β 1-class integrin deficiency in adult hippocampal excitatory neurons (Huang et al., 2006). This physiological disruption is observed despite the absence of a pronounced architectural disruption. Finally, we did not perform behavioral testing to more comprehensively assess neurological function in paxillin-deficient animals. Thus, additional analyses will need to be performed to fully assess the role of these proteins in brain development and function.

MATERIALS AND METHODS

Animals

All animal use was approved by the Institutional Animal Care and Use Committee of SUNY Upstate Medical University (NY, USA). The day of vaginal plug discovery is designated embryonic day 0 (E0) and for consistency we define E21 as day of birth, or postnatal day 0 (P0), regardless of the actual day of birth so as to ensure that the neurons compared in different experimental conditions have been given the same amount of time to differentiate and migrate after labeling (*in utero* electroporation). Floxed paxillin mice were generated by the Gene Targeting and Transgenic Facility of the University of Connecticut (Farmington, CT, USA) for this study (see supplementary Materials and Methods). *Pax^{F/F}* were crossed to *Nestin-Cre*, *NEX-Cre* and *Hic-5* single knockout (*Hic-5^{-/-}*) for genotype analyses (see supplementary Materials and Methods).

Histology

Postnatal mice were first deeply anesthetized by 5% isoflurane inhalation and then transcardial perfusion was performed with Pagano solution [250 mM sucrose, 2.5 mM KCl, 2.5 mM MgCl₂, 25 mM HEPES (pH 7.4)] followed by perfusion with fresh 4% paraformaldehyde/Pagano (PFA/Pagano) fixative solution. Brains were dissected and post-fixed in 4% PFA/Pagano solution for 24 h, then embedded in 10% calf-skin gelatin (Sigma Aldrich) followed by additional fixation in 4% PFA/Pagano for 24 h at 4°C. Embryonic brains were dissected and drop fixed in 4% PFA/Pagano for 1-2 h at room temperature prior to post-fixation and embedding. Brain weights were measured 24 h after fixation and normalized to body weight measured immediately prior to sacrifice.

Immunohistochemistry

Brains were sectioned at 100 μ m using a Vibratome 1000. Free-floating sections were immunostained (O'Dell et al., 2012) using the following primary antibodies: anti-Cux1 (1:50, SantaCruz, sc-13024), anti-Tbr1 (1:500, EMD Millipore, AB2261), anti-Tle4 (1:1000; a kind gift from

Dr Stefano Stifani, McGill University, Canada), anti-Ctip1 (1:500, Abcam, ab19489), anti-Ctip2 (1:500, Abcam, ab18465), anti-BrdU (1:10, DSHB) and anti-paxillin (1:200, rabbit monoclonal; clone Y113, Abcam). Primary antibodies were detected using Alexa Fluor 488-, 555- and 647-conjugated secondary antibodies (1:500, Invitrogen). Hoechst 33342 (2 μ g/ml, Molecular Probes) was used to counterstain nuclei. Histological sections were mounted in antifade media [90% glycerol; 0.5% n-propyl gallate; 20 mM Tris (pH 7.4)] under No.1.5 coverslips (VWR) for subsequent microscopy.

In utero electroporation

In utero electroporation protocols were performed as described previously (Tabata and Nakajima, 2001; Olson et al., 2006). The plasmids used in this study were pCAG-Cre:GFP (1.0 mg/ml) (Addgene #13776) and pCAG-tdTomato (0.5 mg/ml) (O'Dell et al., 2015). To aid injection targeting, 0.01% Fast Green dye (Sigma) was added to the plasmid solution. Electroporations were performed with paddle electrodes using 5 \times 50 ms 50 V pulses with 950 ms interpulse interval with an BTX ECM830 electroporator (Harvard Apparatus).

Imaging and analysis

High-resolution z-series were acquired with a Zeiss LSM 780 laser scanning confocal microscope (Confocal and Two-Photon Imaging Core, SUNY Upstate Medical University, NY, USA) using a Plan-Apochromat 40x/1.4 NA objective. Individual neurons were optically zoomed 2-4 times and z-stacks were acquired at 1 μ m intervals. The length of the leading processes was measured in 3D using the Simple Neurite Tracer Plugin (Longair et al., 2011) within Fiji (Schindelin et al., 2012). Neurite swelling was quantified after z-projection (flattening).

Two-photon live imaging

Embryonic day 13 (E13) embryos were electroporated *ex utero* with a plasmid including CAG-tdTomato (0.4 mg/ml) encoding a red fluorescent protein. After electroporation hemispheres were dissected and cultured medial side down on collagen-coated filters (Transwell-COL, Corning) in DMEM-F12 medium supplemented with 2% B27, 1% G5 and 1 \times pen-strep. After 2 DIV, hemispheres were imaged using a ThorA multiphoton microscope (Thorlabs) equipped with an Olympus 20 \times 1.0 NA water-immersion objective and an InSight Deep See Ti:sapphire laser (Spectra Physics) tuned to 970 nm for excitation. Explants were superfused with warmed oxygenated media during the imaging period. Z-series are acquired at 10 min intervals through >150 μ m of tissue. A minimum of 10 neurons from approximately three different imaged explants, per genotype or condition, were analyzed. Image concatenation, registration and 4D visualization was performed on a HPZ820 workstation and neurites were traced in 3D using the Simple Neurite Tracer Plugin within FIJI.

Western blot analysis

Embryonic cortices were isolated and the meninges were removed. Cortices were triturated in RIPA buffer (50 mM Tris-HCl; 1% NP-40; 0.25% Na-deoxycholate; 150 mM NaCl; 1 mM EDTA, pH 7.4) with protease inhibitors (P8340 Protease Inhibitor Cocktail, Sigma) and phosphatase inhibitors (1 mM Na₃VO₄; 1 mM NaF) followed by brief sonication. Cortical lysates were then separated by standard SDS-PAGE under reducing conditions using Laemmli loading buffer with 1.25% β -mercaptoethanol. Following separation, proteins were transferred to PVDF Immobilon-FL membrane (EMD Millipore). Membranes were blocked with Odyssey blocking buffer (LI-COR Biosciences) for 1 h at room temperature followed by overnight incubation with primary antibodies at 4°C. The following primary antibodies were used: anti-paxillin (1:500, SantaCruz, sc-5574), anti-Hic-5 (1:500, BD Biosciences, 611164), anti-FAK (1:800, BD Biosciences, 610088), anti-pY397FAK (1:1000, Invitrogen, 44-625G), anti-GAPDH (1:2000, UBPBio, Y1040), anti- α -tubulin (1:2000, Sigma, T5168) were used as loading controls. Appropriate secondary antibodies IRDye 800CW and IRDye 680RD (LICOR Biosciences) were used. Probed blots were scanned using an infrared imager (Odyssey CLx, LI-COR Biosciences).

RT-qPCR

Fluorescence-activated cell (FAC) sorting of Eomes-eGFP positive cells and RNA isolation were performed as described previously (Cameron et al., 2012). QuantiTect Reverse Transcription Kit (Qiagen) was used to synthesize cDNA. qPCR were performed using the LightCycler 480 SYBR Green I Master Mix (Roche) under standard conditions on a CFX384 thermal cycler (Bio-Rad). Forward and reverse primers for each gene targeted distinct exons, eliminating the possibility that the quantified amplicons were derived from a chromosomal template rather than reverse transcribed mRNA. The following primers were used for qPCR: *Pxn* forward, 5'-tcttaccacactggaacca-3'; *Pxn* reverse, 5'-cactgcttcagctccagta-3'; *Hic-5* forward, 5'-gtaaccaacccatccgacac-3'; *Hic-5* reverse, 5'-gctgagcattggaatgttt-3'; *Lpxn* forward, 5'-aagaagccatactgcccga-3'; *Lpxn* reverse, 5'-ggctggggacagaatctatg-3'; *G6pdh* forward, 5'-ggcaagctctcaaaacttg-3'; *G6pdh* reverse, 5'-agagcccccataatgct-3'. $2^{-\Delta\Delta CT}$ values were used to calculate relative expression (Livak and Schmittgen, 2001) and are presented as mean \pm s.e.m. The Affymetrix microarray study methodology (Cameron et al., 2012) and *in situ* hybridization analysis are described in more detail in the supplementary Materials and Methods.

Statistical analysis

SigmaPlot 11.0 (Systat Software) was used for statistical analysis. Student's *t*-test was used for pairwise comparisons. For migration speed, leading process length and swelling quantification, at least 15 cells from a minimum of three animals, were quantified in each group. For box-and-whisker data, horizontal black line represents median; horizontal red line represents mean; box represents 25th to 75th percentile; whisker represents 10th to 90th percentile; and circles represent outliers. Numbers on *x*-axis of the box-whisker represents individual animals. Dashed white lines outline the pial surface. Error bars represent standard error of the mean (s.e.m.).

Acknowledgements

We thank Joshua Enck, Aditya Kaliath and members of the Olson lab for assistance and valuable input on the project. We are grateful to Dr Stefano Stifani for providing the Tie4 antibody.

Competing interests

The authors declare no competing or financial interests.

Author contributions

Conceptualization: M.R., C.E.T., E.C.O.; Methodology: M.R., J.B., D.C., C.E.T., E.C.O.; Formal analysis: M.R.; Investigation: M.R., E.C.O.; Writing - original draft: M.R., E.C.O.; Writing - review & editing: M.R., J.B., D.C., C.E.T., E.C.O.; Supervision: E.C.O.; Project administration: E.C.O.; Funding acquisition: C.E.T., E.C.O.

Funding

This work was supported by the National Institutes of Health (R01 NS066071 to E.C.O. and C.E.T.; R01 CA163296 and R01 GM047607 to C.E.T.). Deposited in PMC for release after 12 months.

Supplementary information

Supplementary information available online at <http://dev.biologists.org/lookup/doi/10.1242/dev.147934.supplemental>

References

Anton, E. S., Kreidberg, J. A. and Rakic, P. (1999). Distinct functions of alpha3 and alpha(v) integrin receptors in neuronal migration and laminar organization of the cerebral cortex. *Neuron* **22**, 277-289.

Bahi-Buisson, N., Poirier, K., Fourniol, F., Saillour, Y., Valence, S., Lebrun, N., Hully, M., Bianco, C. F., Bodaert, N., Elie, C. et al. (2014). The wide spectrum of tubulinopathies: what are the key features for the diagnosis? *Brain* **137**, 1676-1700.

Bartholomä, A. and Nave, K.-A. (1994). NEX-1: a novel brain-specific helix-loop-helix protein with autoregulation and sustained expression in mature cortical neurons. *Mech. Dev.* **48**, 217-228.

Beggs, H. E., Schahin-Reed, D., Zang, K., Goebbels, S., Nave, K.-A., Gorski, J., Jones, K. R., Sretavan, D. and Reichardt, L. F. (2003). FAK deficiency in cells contributing to the basal lamina results in cortical abnormalities resembling congenital muscular dystrophies. *Neuron* **40**, 501-514.

Bellis, S. L., Miller, J. T. and Turner, C. E. (1995). Characterization of tyrosine phosphorylation of paxillin *in vitro* by focal adhesion kinase. *J. Biol. Chem.* **270**, 17437-17441.

Belvindrah, R., Graus-Porta, D., Goebbels, S., Nave, K.-A. and Muller, U. (2007). Beta1 integrins in radial glia but not in migrating neurons are essential for the formation of cell layers in the cerebral cortex. *J. Neurosci.* **27**, 13854-13865.

Birge, R. B., Fajardo, J. E., Reichman, C., Shoelson, S. E., Songyang, Z., Cantley, L. C. and Hanafusa, H. (1993). Identification and characterization of a high-affinity interaction between v-Crk and tyrosine-phosphorylated paxillin in CT10-transformed fibroblasts. *Mol. Cell. Biol.* **13**, 4648-4656.

Block, M. R., Badowski, C., Millon-Fremillon, A., Bouvard, D., Bouin, A. P., Faurobert, E., Gerber-Scokaert, D., Planus, E. and Albignat-Rizo, C. (2008). Podosome-type adhesions and focal adhesions, so alike yet so different. *Eur. J. Cell Biol.* **87**, 491-506.

Brown, M. C. and Turner, C. E. (2004). Paxillin: adapting to change. *Physiol. Rev.* **84**, 1315-1339.

Bulfone, A., Smiga, S. M., Shimamura, K., Peterson, A., Puelles, L. and Rubenstein, J. L. R. (1995). T-brain-1: a homolog of Brachyury whose expression defines molecularly distinct domains within the cerebral cortex. *Neuron* **15**, 63-78.

Burridge, K., Fath, K., Kelly, T., Nuckolls, G. and Turner, C. (1988). Focal adhesions: transmembrane junctions between the extracellular matrix and the cytoskeleton. *Annu. Rev. Cell Biol.* **4**, 487-525.

Cameron, R. S. and Rakic, P. (1994). Identification of membrane proteins that comprise the plasmalemmal junction between migrating neurons and radial glial cells. *J. Neurosci.* **14**, 3139-3155.

Cameron, D. A., Middleton, F. A., Chenn, A. and Olson, E. C. (2012). Hierarchical clustering of gene expression patterns in the Eomes+lineage of excitatory neurons during early neocortical development. *BMC Neurosci.* **13**, 90.

Chai, X., Fan, L., Shao, H., Lu, X., Zhang, W., Li, J., Wang, J., Chen, S., Frotscher, M. and Zhao, S. (2015). Reelin induces branching of neurons and radial glial cells during corticogenesis. *Cereb. Cortex* **25**, 3640-3653.

Chen, L., Liao, G., Waclaw, R. R., Burns, K. A., Linquist, D., Campbell, K., Zheng, Y. and Kuan, C.-Y. (2007). Rac1 controls the formation of midline commissures and the competency of tangential migration in ventral telencephalic neurons. *J. Neurosci.* **27**, 3884-3893.

Cooper, J. A. (2013). Cell biology in neuroscience: mechanisms of cell migration in the nervous system. *J. Cell Biol.* **202**, 725-734.

Cousin, B., Leloup, C., Pénicaud, L. and Price, J. (1997). Developmental changes in integrin beta-subunits in rat cerebral cortex. *Neurosci. Lett.* **234**, 161-165.

Deakin, N. O. and Turner, C. E. (2008). Paxillin comes of age. *J. Cell Sci.* **121**, 2435-2444.

Deakin, N. O. and Turner, C. E. (2011). Distinct roles for paxillin and Hic-5 in regulating breast cancer cell morphology, invasion, and metastasis. *Mol. Biol. Cell* **22**, 327-341.

Deakin, N. O. and Turner, C. E. (2014). Paxillin inhibits HDAC6 to regulate microtubule acetylation, Golgi structure, and polarized migration. *J. Cell Biol.* **206**, 395-413.

Deramaudt, T. B., Dujardin, D., Noulet, F., Martin, S., Vauchelles, R., Takeda, K. and Ronde, P. (2014). Altering FAK-paxillin interactions reduces adhesion, migration and invasion processes. *PLoS ONE* **9**, e92059.

Des Portes, V., Francis, F., Pinard, J.-M., Desguerre, I., Moutard, M.-L., Snoeck, I., Meiners, L. C., Capron, F., Cusmai, R., Ricci, S. et al. (1998). doublecortin is the major gene causing X-linked subcortical laminar heterotopia (SCLH). *Hum. Mol. Genet.* **7**, 1063-1070.

Dobyns, W. B., Reiner, O., Carrozzo, R. and Ledbetter, D. H. (1993). Lissencephaly. A human brain malformation associated with deletion of the LIS1 gene located at chromosome 17p13. *JAMA* **270**, 2838-2842.

Dulabon, L., Olson, E. C., Taglienti, M. G., Eisenhuth, S., McGrath, B., Walsh, C. A., Kreidberg, J. A. and Anton, E. S. (2000). Reelin binds alpha3beta1 integrin and inhibits neuronal migration. *Neuron* **27**, 33-44.

Elias, L. A. B., Wang, D. D. and Kriegstein, A. R. (2007). Gap junction adhesion is necessary for radial migration in the neocortex. *Nature* **448**, 901-907.

Englund, C., Fink, A., Lau, C., Pham, D., Daza, R. A., Bulfone, A., Kowalczyk, T. and Hevner, R. F. (2005). Pax6, Tbr2, and Tbr1 are expressed sequentially by radial glia, intermediate progenitor cells, and postmitotic neurons in developing neocortex. *J. Neurosci.* **25**, 247-251.

Franco, S. J. and Müller, U. (2011). Extracellular matrix functions during neuronal migration and lamination in the mammalian central nervous system. *Dev. Neurobiol.* **71**, 889-900.

Franco, S. J., Martinez-Garay, I., Gil-Sanz, C., Harkins-Perry, S. R. and Müller, U. (2011). Reelin regulates cadherin function via Dab1/Rap1 to control neuronal migration and lamination in the neocortex. *Neuron* **69**, 482-497.

Fushiki, S., Perez Velazquez, J. L., Zhang, L., Bechberger, J. F., Carlen, P. L. and Naus, C. C. (2003). Changes in neuronal migration in neocortex of connexin43 null mutant mice. *J. Neuropathol. Exp. Neurol.* **62**, 304-314.

Gdalyahu, A., Ghosh, I., Levy, T., Sapir, T., Sapoznik, S., Fishler, Y., Azoulai, D. and Reiner, O. (2004). DCX, a new mediator of the JNK pathway. *EMBO J.* **23**, 823-832.

Gleeson, J. G., Allen, K. M., Fox, J. W., Lamperti, E. D., Berkovic, S., Scheffer, I., Cooper, E. C., Dobyns, W. B., Minnerath, S. R., Ross, M. E. et al. (1998). Doublecortin, a brain-specific gene mutated in human X-linked lissencephaly and double cortex syndrome, encodes a putative signaling protein. *Cell* **92**, 63-72.

- Gomez, T. M., Roche, F. K. and Letourneau, P. C. (1996). Chick sensory neuronal growth cones distinguish fibronectin from laminin by making substratum contacts that resemble focal contacts. *J. Neurobiol.* **29**, 18-34.
- Goreczny, G. J., Ouderkirch-Pecone, J. L., Olson, E. C., Krendel, M. and Turner, C. E. (2016). Hic-5 remodeling of the stromal matrix promotes breast tumor progression. *Oncogene* **36**, 2693-2703.
- Graus-Porta, D., Blaess, S., Senften, M., Littlewood-Evans, A., Damsky, C., Huang, Z., Orban, P., Klein, R., Schittny, J. C. and Muller, U. (2001). Beta1-class integrins regulate the development of laminae and folia in the cerebral and cerebellar cortex. *Neuron* **31**, 367-379.
- Hagel, M., George, E. L., Kim, A., Tamimi, R., Opitz, S. L., Turner, C. E., Imamoto, A. and Thomas, S. M. (2002). The adaptor protein paxillin is essential for normal development in the mouse and is a critical transducer of fibronectin signaling. *Mol. Cell. Biol.* **22**, 901-915.
- Hevner, R. F., Shi, L., Justice, N., Hsueh, Y.-P., Sheng, M., Smiga, S., Bulfone, A., Goffinet, A. M., Campagnoni, A. T. and Rubenstein, J. L. R. (2001). Tbr1 regulates differentiation of the preplate and layer 6. *Neuron* **29**, 353-366.
- Hildebrand, J. D., Schaller, M. D. and Parsons, J. T. (1995). Paxillin, a tyrosine phosphorylated focal adhesion-associated protein binds to the carboxyl terminal domain of focal adhesion kinase. *Mol. Biol. Cell* **6**, 637-647.
- Huang, Z., Shimazu, K., Woo, N. H., Zang, K., Müller, U., Lu, B. and Reichardt, L. F. (2006). Distinct roles of the beta 1-class integrins at the developing and the mature hippocampal excitatory synapse. *J. Neurosci.* **26**, 11208-11219.
- Jossin, Y. and Cooper, J. A. (2011). Reelin, Rap1 and N-cadherin orient the migration of multipolar neurons in the developing neocortex. *Nat. Neurosci.* **14**, 697-703.
- Kawauchi, T. (2015). Cellular insights into cerebral cortical development: focusing on the locomotion mode of neuronal migration. *Front. Cell Neurosci.* **9**, 394.
- Kawauchi, T., Chihama, K., Nabeshima, Y. and Hoshino, M. (2003). The in vivo roles of STEF/Tiam1, Rac1 and JNK in cortical neuronal migration. *EMBO J.* **22**, 4190-4201.
- Kawauchi, T., Chihama, K., Nishimura, Y. V., Nabeshima, Y. and Hoshino, M. (2005). MAP1B phosphorylation is differentially regulated by Cdk5/p35, Cdk5/p25, and JNK. *Biochem. Biophys. Res. Commun.* **331**, 50-55.
- Kim-Kaneyama, J.-R., Takeda, N., Sasai, A., Miyazaki, A., Sata, M., Hirabayashi, T., Shibayama, M., Yamada, G. and Nose, K. (2011). Hic-5 deficiency enhances mechanosensitive apoptosis and modulates vascular remodeling. *J. Mol. Cell. Cardiol.* **50**, 77-86.
- Kriegstein, A. R. and Noctor, S. C. (2004). Patterns of neuronal migration in the embryonic cortex. *Trends Neurosci.* **27**, 392-399.
- Lipsky, B. P., Beals, C. R. and Staunton, D. E. (1998). Leupaxin is a novel LIM domain protein that forms a complex with PYK2. *J. Biol. Chem.* **273**, 11709-11713.
- Livak, K. J. and Schmittgen, T. D. (2001). Analysis of relative gene expression data using real-time quantitative PCR and the 2(-Delta Delta C(T)) Method. *Methods* **25**, 402-408.
- Longair, M. H., Baker, D. A. and Armstrong, J. D. (2011). Simple Neurite Tracer: open source software for reconstruction, visualization and analysis of neuronal processes. *Bioinformatics* **27**, 2453-2454.
- Lo Nigro, C., Chong, C. S., Smith, A. C. M., Dobyns, W. B., Carrozzo, R. and Ledbetter, D. H. (1997). Point mutations and an intragenic deletion in LIS1, the lissencephaly causative gene in isolated lissencephaly sequence and Miller-Dieker syndrome. *Hum. Mol. Genet.* **6**, 157-164.
- Malatesta, P., Hartfuss, E. and Götz, M. (2000). Isolation of radial glial cells by fluorescent-activated cell sorting reveals a neuronal lineage. *Development* **127**, 5253-5263.
- Marchetti, G., Escuin, S., Van Der Flier, A., De Arcangelis, A., Hynes, R. O. and Georges-Labouesse, E. (2010). Integrin alpha5beta1 is necessary for regulation of radial migration of cortical neurons during mouse brain development. *Eur. J. Neurosci.* **31**, 399-409.
- Matsuda, T. and Cepko, C. L. (2007). Controlled expression of transgenes introduced by in vivo electroporation. *Proc. Natl. Acad. Sci. USA* **104**, 1027-1032.
- Menegon, A., Burgaya, F., Baudot, P., Dunlap, D. D., Girault, J.-A. and Valtorta, F. (1999). FAK+ and PYK2/CAKbeta, two related tyrosine kinases highly expressed in the central nervous system: similarities and differences in the expression pattern. *Eur. J. Neurosci.* **11**, 3777-3788.
- Miyamoto, Y., Torii, T., Yamamori, N., Eguchi, T., Nagao, M., Nakamura, K., Tanoue, A. and Yamauchi, J. (2012). Paxillin is the target of c-Jun N-terminal kinase in Schwann cells and regulates migration. *Cell. Signal.* **24**, 2061-2069.
- Molyneaux, B. J., Goff, L. A., Brettler, A. C., Chen, H.-H., Brown, J. R., Hrvatin, S., Rinn, J. L. and Arlotta, P. (2015). DeCoN: genome-wide analysis of in vivo transcriptional dynamics during pyramidal neuron fate selection in neocortex. *Neuron* **85**, 275-288.
- Myers, J. P. and Gomez, T. M. (2011). Focal adhesion kinase promotes integrin adhesion dynamics necessary for chemotropic turning of nerve growth cones. *J. Neurosci.* **31**, 13585-13595.
- Nadarajah, B., Jones, A. M., Evans, W. H. and Parnavelas, J. G. (1997). Differential expression of connexins during neocortical development and neuronal circuit formation. *J. Neurosci.* **17**, 3096-3111.
- Nadarajah, B., Brunstrom, J. E., Grutzendler, J., Wong, R. O. L. and Pearlman, A. L. (2001). Two modes of radial migration in early development of the cerebral cortex. *Nat. Neurosci.* **4**, 143-150.
- Nadarajah, B., Alifragis, P., Wong, R. O. L. and Parnavelas, J. G. (2003). Neuronal migration in the developing cerebral cortex: observations based on real-time imaging. *Cereb. Cortex* **13**, 607-611.
- Nichols, A. J., O'Dell, R. S., Powrozek, T. A. and Olson, E. C. (2013). Ex utero electroporation and whole hemisphere explants: a simple experimental method for studies of early cortical development. *J. Vis. Exp.* **74**, e50271.
- Nieto, M., Monuki, E. S., Tang, H., Imitola, J., Haubst, N., Khoury, S. J., Cunningham, J., Gotz, M. and Walsh, C. A. (2004). Expression of Cux-1 and Cux-2 in the subventricular zone and upper layers II-IV of the cerebral cortex. *J. Comp. Neurol.* **479**, 168-180.
- Niewmierzycka, A., Mills, J., St-Arnaud, R., Dedhar, S. and Reichardt, L. F. (2005). Integrin-linked kinase deletion from mouse cortex results in cortical lamination defects resembling cobblestone lissencephaly. *J. Neurosci.* **25**, 7022-7031.
- Noctor, S. C., Martinez-Cerdeno, V., Ivic, L. and Kriegstein, A. R. (2004). Cortical neurons arise in symmetric and asymmetric division zones and migrate through specific phases. *Nat. Neurosci.* **7**, 136-144.
- O'Dell, R. S., Ustine, C. J. M., Cameron, D. A., Lawless, S. M., Williams, R. M., Zipfel, W. R. and Olson, E. C. (2012). Layer 6 cortical neurons require Reelin-Dab1 signaling for cellular orientation, Golgi deployment, and directed neurite growth into the marginal zone. *Neural Dev.* **7**, 25.
- O'Dell, R. S., Cameron, D. A., Zipfel, W. R. and Olson, E. C. (2015). Reelin prevents apical neurite retraction during terminal translocation and dendrite initiation. *J. Neurosci.* **35**, 10659-10674.
- Olson, E. C., Kim, S. and Walsh, C. A. (2006). Impaired neuronal positioning and dendritogenesis in the neocortex after cell-autonomous Dab1 suppression. *J. Neurosci.* **26**, 1767-1775.
- O'Rourke, N. A., Dailey, M. E., Smith, S. J. and McConnell, S. K. (1992). Diverse migratory pathways in the developing cerebral cortex. *Science* **258**, 299-302.
- Rakic, P. (1972). Mode of cell migration to the superficial layers of fetal monkey neocortex. *J. Comp. Neurol.* **145**, 61-83.
- Renaudin, A., Lehmann, M., Girault, J.-A. and McKerracher, L. (1999). Organization of point contacts in neuronal growth cones. *J. Neurosci. Res.* **55**, 458-471.
- Rico, B., Beggs, H. E., Schahin-Reed, D., Kimes, N., Schmidt, A. and Reichardt, L. F. (2004). Control of axonal branching and synapse formation by focal adhesion kinase. *Nat. Neurosci.* **7**, 1059-1069.
- Robles, E. and Gomez, T. M. (2006). Focal adhesion kinase signaling at sites of integrin-mediated adhesion controls axon pathfinding. *Nat. Neurosci.* **9**, 1274-1283.
- Salgia, R., Uemura, N., Okuda, K., Li, J.-L., Pisick, E., Sattler, M., De Jong, R., Druker, B., Heisterkamp, N., Chen, L. B. et al. (1995). CRKL links p210BCR/ABL with paxillin in chronic myelogenous leukemia cells. *J. Biol. Chem.* **270**, 29145-29150.
- Schaller, M. D. and Parsons, J. T. (1995). pp125FAK-dependent tyrosine phosphorylation of paxillin creates a high-affinity binding site for Crk. *Mol. Cell. Biol.* **15**, 2635-2645.
- Schindelin, J., Arganda-Carreras, I., Frise, E., Kaynig, V., Longair, M., Pietzsch, T., Preibisch, S., Rueden, C., Saalfeld, S., Schmid, B. et al. (2012). Fiji: an open-source platform for biological-image analysis. *Nat. Methods* **9**, 676-682.
- Schmid, R. S. and Anton, E. S. (2003). Role of integrins in the development of the cerebral cortex. *Cereb. Cortex* **13**, 219-224.
- Schmid, R. S., Shelton, S., Stanco, A., Yokota, Y., Kreidberg, J. A. and Anton, E. S. (2004). alpha3beta1 integrin modulates neuronal migration and placement during early stages of cerebral cortical development. *Development* **131**, 6023-6031.
- Sekine, K., Kawauchi, T., Kubo, K., Honda, T., Herz, J., Hattori, M., Kinashi, T. and Nakajima, K. (2012). Reelin controls neuronal positioning by promoting cell-matrix adhesion via inside-out activation of integrin alpha5beta1. *Neuron* **76**, 353-369.
- Sero, J. E., Thodeti, C. K., Mammoto, A., Bakal, C., Thomas, S. and Ingber, D. E. (2011). Paxillin mediates sensing of physical cues and regulates directional cell motility by controlling lamellipodia positioning. *PLoS ONE* **6**, e28303.
- Shibanuma, M., Kim-Kaneyama, J.-R., Sato, S. and Nose, K. (2004). A LIM protein, Hic-5, functions as a potential coactivator for Sp1. *J. Cell. Biochem.* **91**, 633-645.
- Stocker, A. M. and Chenn, A. (2015). The role of adherens junctions in the developing neocortex. *Cell Adh. Migr.* **9**, 167-174.
- Tabata, H. and Nakajima, K. (2001). Efficient in utero gene transfer system to the developing mouse brain using electroporation: visualization of neuronal migration in the developing cortex. *Neuroscience* **103**, 865-872.
- Tabata, H. and Nakajima, K. (2003). Multipolar migration: the third mode of radial neuronal migration in the developing cerebral cortex. *J. Neurosci.* **23**, 9996-10001.
- Tahirovic, S., Hellal, F., Neukirchen, D., Hindges, R., Garvalov, B. K., Flynn, K. C., Stradal, T. E., Chrostek-Grashoff, A., Brakebusch, C. and Bradke, F. (2010). Rac1 regulates neuronal polarization through the WAVE complex. *J. Neurosci.* **30**, 6930-6943.

- Takahashi, T., Goto, T., Miyama, S., Nowakowski, R. S. and Caviness, V. S., Jr** (1999). Sequence of neuron origin and neocortical laminar fate: relation to cell cycle of origin in the developing murine cerebral wall. *J. Neurosci.* **19**, 10357-10371.
- Tronche, F., Kellendonk, C., Kretz, O., Gass, P., Anlag, K., Orban, P. C., Bock, R., Klein, R. and Schütz, G.** (1999). Disruption of the glucocorticoid receptor gene in the nervous system results in reduced anxiety. *Nat. Genet.* **23**, 99-103.
- Tumbarello, D. A. and Turner, C. E.** (2007). Hic-5 contributes to epithelial-mesenchymal transformation through a RhoA/ROCK-dependent pathway. *J. Cell. Physiol.* **211**, 736-747.
- Valiente, M., Ciceri, G., Rico, B. and Marin, O.** (2011). Focal adhesion kinase modulates radial glia-dependent neuronal migration through connexin-26. *J. Neurosci.* **31**, 11678-11691.
- Wiegrefe, C., Simon, R., Peschkes, K., Kling, C., Strehle, M., Cheng, J., Srivatsa, S., Liu, P., Jenkins, N. A., Copeland, N. G. et al.** (2015). Bcl11a (Ctip1) controls migration of cortical projection neurons through regulation of Sema3c. *Neuron* **87**, 311-325.
- Wu, S.-X., Goebbels, S., Nakamura, K., Kometani, K., Minato, N., Kaneko, T., Nave, K.-A. and Tamamaki, N.** (2005). Pyramidal neurons of upper cortical layers generated by NEX-positive progenitor cells in the subventricular zone. *Proc. Natl. Acad. Sci. USA* **102**, 17172-17177.
- Yao, J., Liu, Y., Husain, J., Lo, R., Palaparti, A., Henderson, J. and Stifani, S.** (1998). Combinatorial expression patterns of individual TLE proteins during cell determination and differentiation suggest non-redundant functions for mammalian homologs of Drosophila Groucho. *Dev. Growth Differ.* **40**, 133-146.
- Yi, Y.-H., Chang, Y.-S., Lin, C.-H., Lew, T.-S., Tang, C.-Y., Tseng, W.-L., Tseng, C.-P. and Lo, S. J.** (2012). Integrin-mediated membrane blebbing is dependent on sodium-proton exchanger 1 and sodium-calcium exchanger 1 activity. *J. Biol. Chem.* **287**, 10316-10324.
- Zaidel-Bar, R., Cohen, M., Addadi, L. and Geiger, B.** (2004). Hierarchical assembly of cell-matrix adhesion complexes. *Biochem. Soc. Trans.* **32**, 416-420.